New physics in $b \to se^+e^-$: A model independent analysis

Suman Kumbhakar

Indian Institute of Science
Bangalore

Based on Nucl.Phys.B 967 (2021) 115419; arXiv:2011.14668
with A K Alok (IIT Jodhpur), J. Saini (IIT Jodhpur) and S Uma Sankar (IIT Bombay)

The XXVIII SUSY 2021, Beijing

Outline

- Lepton Flavor Universality and its violation in $b \to s\ell^+\ell^-$
- New Physics solutions in $b \to se^+e^-$
- Methods to discriminate the new physics scenarios
- Conclusions

The Standard Model

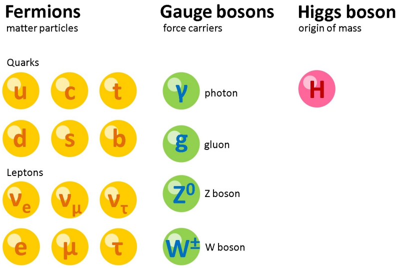

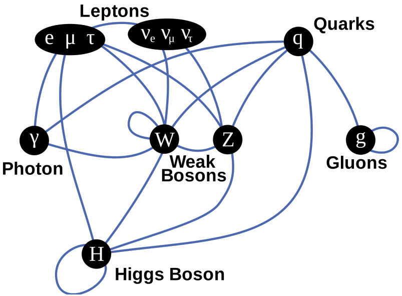

$\Longrightarrow$ The SM becomes highly successful after the Higgs discovery in 2012.
$\Longrightarrow$ All interactions are gauge interactions.
$\Longrightarrow$ The gauge interactions are identical for three generations/ flavors.

Lepton Flavor Universality

Testing LFU through flavor ratios

$$R_K = \frac{Br(B \to K\mu^+\mu^-)}{Br(B \to Ke^+e^-)} \quad R_{K^*} = \frac{Br(B \to K^*\mu^+\mu^-)}{Br(B \to K^*e^+e^-)}$$

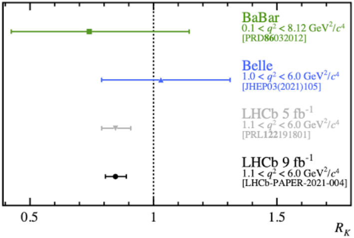

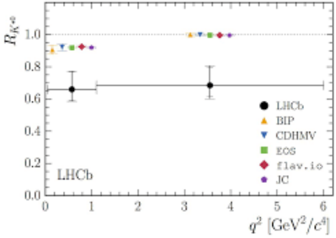

- Measured values are $\sim 2.5 - 3.1\sigma$ lower than the SM prediction.

Violation of LFU $\Longrightarrow$ Hint of new physics

Additional measurements on the branching ratio of $B_s \to \phi\mu^+\mu^-$ and the angular observables in $B \to (K, K^*)\mu^+\mu^-$. [arXiv:1506.08777, arXiv:2003.04831]
Deviation at the level of $3 - 3.5\sigma$ in $Br(B_s \to \phi\mu^+\mu^-)$ and P_5'.
These are subject to significant hadronic uncertainties dominated by undermined power corrections. see e.g. T Hurth et al., arXiv:2006.04213

The SM Effective Hamiltonian

Effective Hamiltonian for $b \to s\ell^+\ell^-$ process is given by

$$\mathcal{H}^{\rm SM} = -\frac{4G_F}{\sqrt{2}\pi} V_{ts}^* V_{tb} \left[\sum_{i=1}^{6} C_i(\mu)\mathcal{O}_i(\mu) + C_7 \frac{e}{16\pi^2} [\bar{s}\sigma_{\mu\nu}(m_s P_L + m_b P_R) b] F^{\mu\nu} \right.$$
$$\left. + C_9 \frac{\alpha_{em}}{4\pi} (\bar{s}\gamma^\mu P_L b)(\bar{\ell}\gamma_\mu \ell) + C_{10} \frac{\alpha_{em}}{4\pi} (\bar{s}\gamma^\mu P_L b)(\bar{\ell}\gamma_\mu \gamma_5 \ell) \right],$$

where G_F is the Fermi constant, V_{ts} and V_{tb} are the Cabibbo-Kobayashi-Maskawa (CKM) matrix elements and $P_{L,R} = (1 \mp \gamma^5)/2$ are the projection operators. The effect of the operators $\mathcal{O}_i$, $i = 1-6, 8$ can be embedded in the redefined effective Wilson coefficients (WCs) as $C_7(\mu) \to C_7^{\rm eff}(\mu, q^2)$ and $C_9(\mu) \to C_9^{\rm eff}(\mu, q^2)$.

New Physics only in $b \to s\mu^+\mu^-$

New Physics in the form of vector and axial vector

$$\mathcal{H}_{\rm NP} = -\frac{\alpha_{\rm em} G_F}{\sqrt{2}\pi} V_{ts}^* V_{tb} \Big[C_9^{\rm NP} (\bar{s}\gamma^\mu P_L b)(\overline{\mu}\gamma_\mu \mu) + C_{10}^{\rm NP} (\bar{s}\gamma^\mu P_L b)(\overline{\mu}\gamma_\mu\gamma_5 \mu) + C_9^{\prime\rm NP} (\bar{s}\gamma^\mu P_R b)(\overline{\mu}\gamma_\mu \mu) + C_{10}^{\prime\rm NP} (\bar{s}\gamma^\mu P_R b)(\overline{\mu}\gamma_\mu\gamma_5 \mu) \Big] + h.c.$$

Several global fit analysis Alguer et al, arXiv:1903.09578; Alok et al, arXiv:1903.09617; Ciuchini et al, arXiv:1903.09632; Aebischer et al, arXiv:1903.10434; Kowalska et al, arXiv:1903.10932; Arbey et al, arXiv:1904.08399.....

$\Longrightarrow$ A common conclusion: Three distinct NP solutions

(arXiv:1903.09617)

NP scenarios	Best fit value	pull $= \sqrt{\chi^2_{\rm SM} - \chi^2_{\rm min}}$
(I) $C_9^{\rm NP}$	-1.01 ± 0.15	6.9
(II) $C_9^{\rm NP} = -C_{10}^{\rm NP}$	-0.49 ± 0.07	7.0
(III) $C_9^{\rm NP} = -C_9^{\prime\rm NP}$	-1.03 ± 0.15	6.7

$\Longrightarrow$ A possible methods to discriminate between these solutions are discussed in Alok et al, arXiv:2001.04395; Li et al, arXiv:2105.06768

New Physics only in $b \to s e^+ e^-$

The effective Hamiltonian in the presence of vector, axial-vector, scalar, pseudoscalar and tensor NP operators is givem by

$$\mathcal{H}_{eff}(b \to s e^+ e^-) = \mathcal{H}_{SM} + \mathcal{H}^{NP}_{VA} + \mathcal{H}^{NP}_{SP} + \mathcal{H}^{NP}_{T},$$

$$\begin{aligned}
\mathcal{H}^{\rm NP}_{\rm VA} &= -\frac{\alpha_{\rm em} G_F}{\sqrt{2}\pi} V^*_{ts} V_{tb} \Big[C_9^{\rm NP,\,e} (\bar{s}\gamma^\mu P_L b)(\bar{e}\gamma_\mu e) + C_{10}^{\rm NP,\,e} (\bar{s}\gamma^\mu P_L b)(\bar{e}\gamma_\mu \gamma_5 e) \\
&\quad + C_9^{\prime,\,\rm e} (\bar{s}\gamma^\mu P_R b)(\bar{e}\gamma_\mu e) + C_{10}^{\prime,\,\rm e} (\bar{s}\gamma^\mu P_R b)(\bar{e}\gamma_\mu \gamma_5 e) \Big], \\
\mathcal{H}^{\rm NP}_{\rm SP} &= -\frac{\alpha_{\rm em} G_F}{\sqrt{2}\pi} V^*_{ts} V_{tb} \big[C^{\rm e}_{SS} (\bar{s}b)(\bar{e}e) + C^{\rm e}_{SP} (\bar{s}b)(\bar{e}\gamma_5 e) \\
&\quad + C^{\rm e}_{PS} (\bar{s}\gamma_5 b)(\bar{e}e) + C^{\rm e}_{PP} (\bar{s}\gamma_5 b)(\bar{e}\gamma_5 e) \big], \\
\mathcal{H}^{\rm NP}_{\rm T} &= -\frac{\alpha_{\rm em} G_F}{\sqrt{2}\pi} V^*_{ts} V_{tb} \big[C^{\rm e}_{T} (\bar{s}\sigma^{\mu\nu} b)(\bar{e}\sigma_{\mu\nu} e) + C^{\rm e}_{T5} (\bar{s}\sigma^{\mu\nu} b)(\bar{e}\sigma_{\mu\nu}\gamma_5 e) \big]
\end{aligned}$$

Constraints on (Pseudo)-scalar and Tensor operators

Scalar/pseudoscalar NP:

- The scalar NP operators $(\bar{s}b)$ can lead to $B \to K$ but not to $B \to K^*$.
- The pseudo-scalar NP operator $(\bar{s}\gamma_5 b)$ can not lead to $B \to K$ transition.
- Hence scalar or pseudo-scalar NP can not explain R_K and R_{K^*} simultaneously.
- In addition, a tight constraint comes from the upper limit of $Br(B_s \to e^+e^-) < 9.4 \times 10^{-9}$ (at C.L. 90%) [LHCb, arXiv:2003.03999]

$$|C^{\rm e}_{PS}|^2 + |C^{\rm e}_{PP}|^2 \lesssim 0.01$$

.

- However, the experimental measurement of $R_{K^*}^{low}$ and $R_{K^*}^{central}$ lead to

$$120 \lesssim |C^{\rm e}_{PS}|^2 + |C^{\rm e}_{PP}|^2 \lesssim 345, \quad 9 \lesssim |C^{\rm e}_{PS}|^2 + |C^{\rm e}_{PP}|^2 \lesssim 29,$$

- Hence, none of the scalar and pseudo-scalar NP operators can explain the $b \to se^+e^-$ data.

Tensor NP:

- Tensor NP operator is constrained by inclusive $Br(B \to X_s e^+e^-)$ and radiative $b \to s\gamma$. Hiller and Schmaltz, PRD90(2014),054014
- Only tensor NP can not accommodate the recent data on $b \to s\ell^+\ell^-$ transition.

(Axial)-Vector New Physics

$$\chi^2(C_i) = \sum_{\text{all obs.}} \frac{\left(O^{\text{th}}(C_i) - O^{\text{exp}}\right)^2}{\sigma^2_{\text{exp}} + \sigma^2_{\text{th}}}.$$

Measurements included into fit:

- R_K, $R_{K^*}^{low}$ and $R_{K^*}^{central}$ by LHCb and R_{K^*} by the Belle collaboration in $0.045 < q^2 < 1.1$ GeV^2, $1.1 < q^2 < 6.0$ GeV^2 and $15.0 < q^2 < 19.0$ GeV^2 bins for both B^0 and B^+ decay modes,
- $Br(B_s \to e^+e^-) < 9.4 \times 10^{-9}$ at 90% C.L. by the LHCb,
- The differential branching fraction of $B \to K^* e^+ e^-$
- K^* longitudinal polarization fraction by LHCb
- $Br(B \to X_s e^+ e^-)$ by the BaBar cn. in both $1.0 < q^2 < 6.0$ GeV^2 and $14.2 < q^2 < 25.0$ GeV^2 bins
- P_4' and P_5' in $B \to K^* e^+ e^-$ decay by the Belle cn in $1.0 < q^2 < 6.0$ GeV^2 and $14.18 < q^2 < 19.0$ GeV^2 bins

Fitting Methodology:

- We use CERN minimization code `Minuit` library to minimize the χ^2.
- We use `Flavio` package to calculate the theoretical expressions of the observables.
- We perform the minimization in two ways: (A) one NP operator at a time and (B) two similar NP operators at a time.

Allowed NP solutions in form of (Axial)-Vector

Solution	Wilson Coefficient(s)	Best fit value(s)	pull	R_K	$R_{K^*}^{\rm low}$	$R_{K^*}^{\rm central}$
Expt. 1σ range				$[0.784, 0.908]$	$[0.547, 0.773]$	$[0.563, 0.807]$
2D Scenarios						
I	$(C_9^{\rm NP,e}, C_9^{\prime,e})$	$(-3.61, -4.76)$	3.1	0.867 ± 0.050	0.757 ± 0.007	0.625 ± 0.024
II		$(-3.52, 4.29)$	3.4	0.832 ± 0.001	0.798 ± 0.028	0.707 ± 0.090
III	$(C_{10}^{\rm NP,e}, C_{10}^{\prime,e})$	$(3.64, 5.33)$	3.0	0.860 ± 0.015	0.788 ± 0.014	0.645 ± 0.015

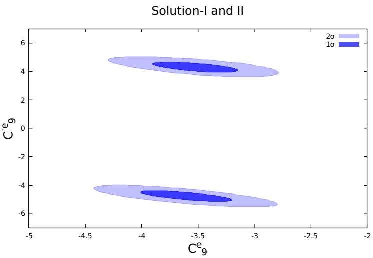

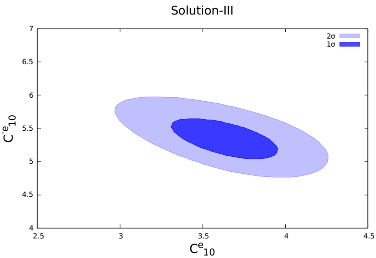

Angular distribution in $B \to K^*(\to K\pi)e^+e^-$

How to distinguish these solutions? $\Longrightarrow$ Angular observables

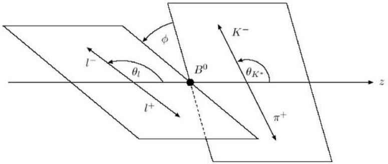

3 angles

Lepton angle θ_l

Kaon angle θ_K

Decay plane angle ϕ

$$\frac{d^4\Gamma}{dq^2\, d\cos\theta_e\, d\cos\theta_K\, d\phi} = \frac{9}{32\pi} I(q^2, \theta_e, \theta_K, \phi),$$

where [Altmannshofer et al JHEP 01 (2009),019]

$$\begin{aligned} I(q^2, \theta_e, \theta_K, \phi) \quad = \quad & I_1^s \sin^2\theta_K + I_1^c \cos^2\theta_K + (I_2^s \sin^2\theta_K + I_2^c \cos^2\theta_K)\cos 2\theta_e \\ & + I_3 \sin^2\theta_K \sin^2\theta_e \cos 2\phi + I_4 \sin 2\theta_K \sin 2\theta_e \cos\phi \\ & + I_5 \sin 2\theta_K \sin\theta_e \cos\phi \\ & + (I_6^s \sin^2\theta_K + I_6^c \cos^2\theta_K)\cos\theta_e + I_7 \sin 2\theta_K \sin\theta_e \sin\phi \\ & + I_8 \sin 2\theta_K \sin 2\theta_e \sin\phi + I_9 \sin^2\theta_K \sin^2\theta_e \sin 2\phi. \end{aligned}$$

Angular observables

CP averaged angular observables:[Descotes-Genon et al JHEP 01 (2013), 048]

$$S_i^{(a)}(q^2) = \frac{I_i^{(a)}(q^2) + \bar{I}_i^{(a)}(q^2)}{d(\Gamma + \bar{\Gamma})/dq^2}.$$

$$A_{FB} = \frac{3}{8}\left(2S_6^s + S_6^c\right), \quad F_L = -S_2^c.$$

$$P_1 = \frac{2S_3}{1-F_L}, \quad P_2 = \frac{S_6^s}{2(1-F_L)}, \quad P_3 = \frac{-S_9}{1-F_L},$$

$$P_4' = \frac{2S_4}{\sqrt{F_L(1-F_L)}}, \quad P_5' = \frac{S_5}{\sqrt{F_L(1-F_L)}}, \quad P_6' = \frac{-S_7}{\sqrt{F_L(1-F_L)}}, \quad P_8' = \frac{-2S_8}{\sqrt{F_L(1-F_L)}}.$$

Distinguishing power of A_{FB}

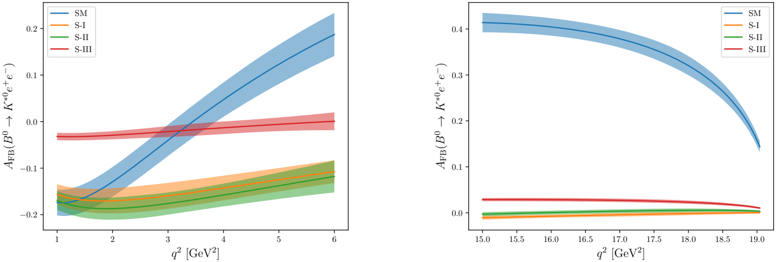

- In low q^2 region, the SM prediction of $A_{FB}(q^2)$ has a zero crossing at ~ 3.5 GeV^2. For the NP solutions, the predictions are negative throughout the low q^2 range. However, the $A_{FB}(q^2)$ curve is almost the same for S-I and S-II whereas for S-III, it is markedly different. Therefore an accurate measurement of q^2 distribution of A_{FB} can discriminate between S-III and the remaining two NP solutions.
- In high q^2 region, the SM prediction of A_{FB} is 0.368 ± 0.018 whereas the predictions for the three solutions are almost zero.

Distinguishing power of F_L

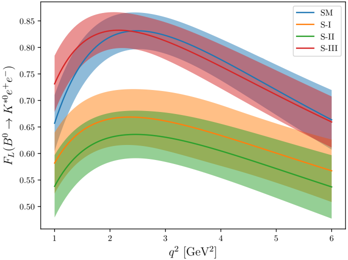

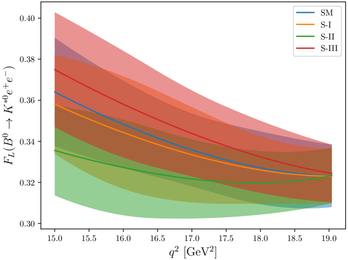

The S-I and S-II scenarios can marginally suppress the value of F_L in low q^2 region compared to the SM whereas for S-III, the predicted value is consistent with the SM. In high q^2 region, F_L for all three scenarios are close to the SM value. Hence F_L cannot discriminate between the allowed V/A solutions.

Most suitable is P_1

Observable	SM	S-I	S-II	S-III
$P_1[1-6]$ GeV^2	-0.113 ± 0.032	0.507 ± 0.064	-0.627 ± 0.035	-0.291 ± 0.034

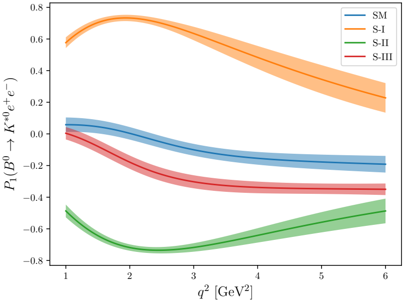

The observable P_1 in the low q^2 region can discriminate between all three NP solutions, particularly S-I and S-II. The sign of P_1 is opposite for these scenarios. Hence an accurate measurement of P_1 can distinguish between S-I and S-II solutions. In fact, measurement of P_1 with an absolute uncertainty of 0.05 can confirm or rule out S-I and S-II solutions by more than 4σ.

Conclusions

- Assuming new physics in $b \to se^+e^-$ transition, we identify the allowed solutions which can explain the deviations in R_K/R_{K^*} measurements.
- We show that none of the (pseudo)-scalar or tensor new physics can explain the $b \to se^+e^-$ data.
- Only three vector/axial-vector new physics solutions (2D fit) can explain the present measurement of R_K/R_{K^*} within 1σ.
- The A_{FB} and F_L in $(B \to K^* e^+ e^-)$ decay have poor ability to discriminate between three new physics solutions.
- In order to discriminate three solutions uniquely, $P_1(B \to K^* e^+ e^-)$ is the most suitable angular observable. If it is measured with a 5% accuracy, P_1 can distinguish all three solutions.

Thank You!

Extra Slides

1D and 2D Fit results

Wilson Coefficient(s)	Best fit value(s)	$\chi^2_{\rm min}$	pull
$C_i = 0$ (SM)	$-$	27.42	
1D Scenarios			
$C_9^{\rm NP,e}$	0.91 ± 0.28	15.21	3.5
$C_{10}^{\rm NP,e}$	-0.86 ± 0.25	12.60	3.8
$C_9^{\prime,e}$	0.24 ± 0.24	26.40	1.0
$C_{10}^{\prime,e}$	-0.17 ± 0.21	26.70	0.8
2D Scenarios			
$(C_9^{\rm NP,e}, C_{10}^{\rm NP,e})$	$(-1.03, -1.42)$	11.57	3.9
$(C_9^{\rm NP,e}, C_9^{\prime,e})$	$(-3.61, -4.76)$ $(-3.52, 4.29)$ $(1.21, -0.54)$	17.65 15.71 12.83	3.1 3.4 3.8
$(C_9^{\rm NP,e}, C_{10}^{\prime,e})$	$(1.21, 0.69)$	12.39	3.9
$(C_9^{\prime,e}, C_{10}^{\rm NP,e})$	$(-0.50, -1.03)$	11.30	4.0
$(C_9^{\prime,e}, C_{10}^{\prime,e})$	$(2.05, 2.33)$ $(-2.63, -1.86)$	10.41 12.71	4.1 3.8
$(C_{10}^{\rm NP,e}, C_{10}^{\prime,e})$	$(3.64, 5.33)$ $(-1.04, 0.38)$ $(4.56, -5.24)$	18.50 11.14 16.58	3.0 4.0 3.3

Table: The best fit values of NP WCs in $b \to s e^+ e^-$ transition for 1D and 2D scenarios. The value of $\chi^2_{\rm SM}$ is 27.42.

Good fit scenarios

Wilson Coefficient(s)	Best fit value(s)	pull	R_K	$R_{K^*}^{\rm low}$	$R_{K^*}^{\rm central}$
Expt. 1σ range			$[0.784, 0.908]$	$[0.547, 0.773]$	$[0.563, 0.807]$
1D Scenarios					
$C_9^{\rm NP,e}$	0.91 ± 0.28	3.5	0.806 ± 0.001	0.883 ± 0.008	0.832 ± 0.009
$C_{10}^{\rm NP,e}$	-0.86 ± 0.25	3.8	0.805 ± 0.005	0.855 ± 0.007	0.778 ± 0.012
2D Scenarios					
$(C_9^{\rm NP,e}, C_{10}^{\rm NP,e})$	$(-1.03, -1.42)$	3.9	0.825 ± 0.011	0.832 ± 0.007	0.745 ± 0.026
$(C_9^{\rm NP,e}, C_9^{\prime,e})$	$(-3.61, -4.76)$	3.1	0.867 ± 0.050	0.757 ± 0.007	0.625 ± 0.024
	$(-3.52, 4.29)$	3.4	0.832 ± 0.001	0.798 ± 0.028	0.707 ± 0.090
	$(1.21, -0.54)$	3.8	0.853 ± 0.001	0.825 ± 0.018	0.701 ± 0.012
$(C_9^{\rm NP,e}, C_{10}^{\prime,e})$	$(1.21, 0.69)$	3.9	0.855 ± 0.004	0.819 ± 0.016	0.691 ± 0.011
$(C_9^{\prime,e}, C_{10}^{\rm NP,e})$	$(-0.50, -1.03)$	4.0	0.844 ± 0.007	0.812 ± 0.012	0.690 ± 0.009
$(C_9^{\prime,e}, C_{10}^{\prime,e})$	$(2.05, 2.33)$	4.1	0.845 ± 0.010	0.808 ± 0.014	0.683 ± 0.029
	$(-2.63, -1.86)$	3.8	0.856 ± 0.020	0.808 ± 0.015	0.684 ± 0.010
$(C_{10}^{\rm NP,e}, C_{10}^{\prime,e})$	$(3.64, 5.33)$	3.0	0.860 ± 0.015	0.788 ± 0.014	0.645 ± 0.015
	$(-1.04, 0.38)$	4.0	0.846 ± 0.004	0.809 ± 0.013	0.686 ± 0.014
	$(4.56, -5.24)$	3.3	0.842 ± 0.004	0.809 ± 0.015	0.685 ± 0.019

Table: The predictions of R_K, $R_{K^*}^{\rm low}$ and $R_{K^*}^{\rm central}$ for the good fit scenarios obtained in previous slide.

Predictions for angular observables

Observable	q^2 bin	SM	S-I	S-II	S-III
P_1	$[1.1, 6]$	-0.113 ± 0.032	0.507 ± 0.064	-0.627 ± 0.035	-0.291 ± 0.034
	$[15, 19]$	-0.623 ± 0.044	-0.602 ± 0.042	-0.609 ± 0.040	-0.700 ± 0.037
P_2	$[1.1, 6]$	0.023 ± 0.090	-0.263 ± 0.020	-0.267 ± 0.021	-0.046 ± 0.030
	$[15, 19]$	0.372 ± 0.013	-0.005 ± 0.004	0.002 ± 0.004	0.027 ± 0.004
P_3	$[1.1, 6]$	0.003 ± 0.008	0.018 ± 0.036	-0.017 ± 0.032	0.002 ± 0.006
	$[15, 19]$	-0.000 ± 0.000	-0.045 ± 0.004	0.045 ± 0.004	-0.000 ± 0.000
P'_4	$[1.1, 6]$	-0.352 ± 0.038	-0.256 ± 0.033	-0.605 ± 0.011	-0.447 ± 0.027
	$[15, 19]$	-0.635 ± 0.008	-0.631 ± 0.008	-0.632 ± 0.008	-0.650 ± 0.008
P'_5	$[1.1, 6]$	-0.440 ± 0.106	0.336 ± 0.060	0.358 ± 0.045	0.487 ± 0.079
	$[15, 19]$	-0.593 ± 0.036	-0.001 ± 0.005	-0.014 ± 0.006	-0.032 ± 0.005
P'_6	$[1.1, 6]$	-0.046 ± 0.102	-0.025 ± 0.053	-0.028 ± 0.066	-0.042 ± 0.093
	$[15, 19]$	-0.002 ± 0.001	-0.002 ± 0.001	-0.002 ± 0.001	-0.002 ± 0.001
P'_8	$[1.1, 6]$	-0.015 ± 0.035	-0.006 ± 0.032	0.012 ± 0.027	-0.009 ± 0.023
	$[15, 19]$	0.001 ± 0.000	0.036 ± 0.002	-0.036 ± 0.003	0.000 ± 0.000

Table: Average values of $P_{1,2,3}$ and $P'_{4,5,6,8}$ in $B \to K^* e^+ e^-$ decay for the three allowed V/A NP solutions as well as for the SM.

$P_1(q^2)$ and $P_2(q^2)$

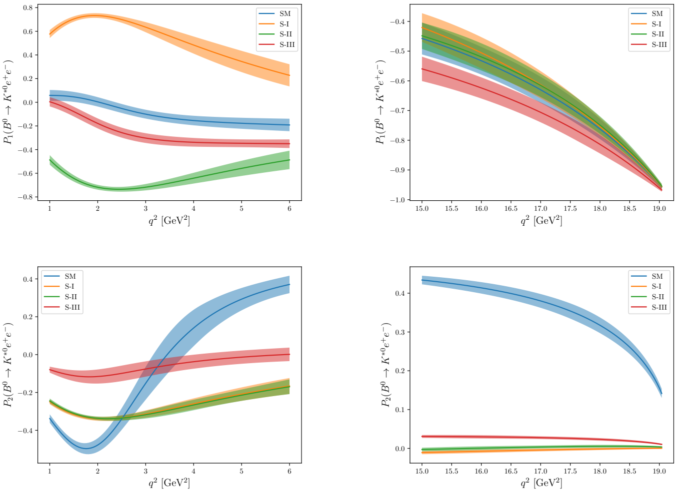

$P_3(q^2)$ and $P_4(q^2)$

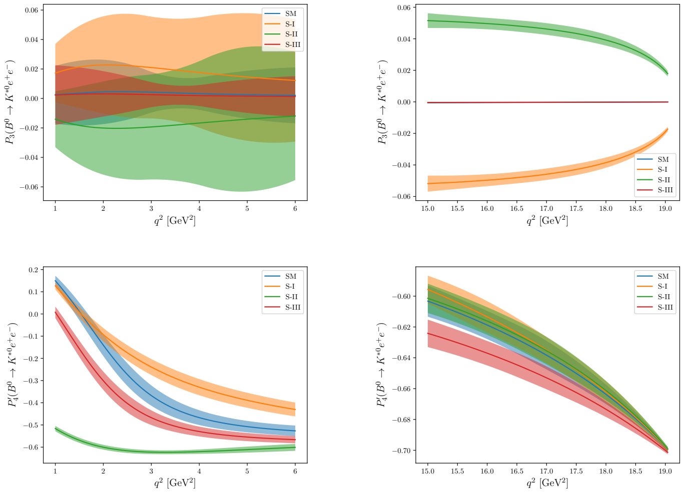

$P_5'(q^2)$ and $P_6'(q^2)$

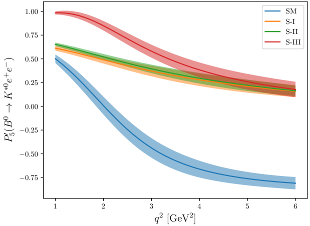

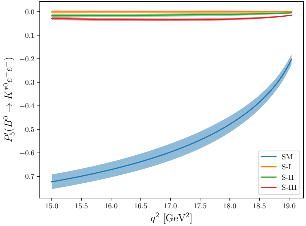

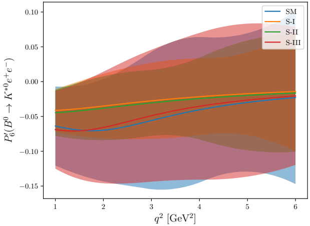

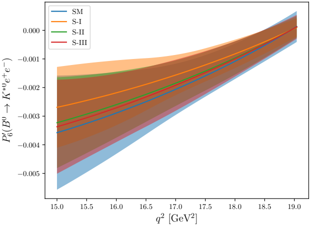

$P_8(q^2)$

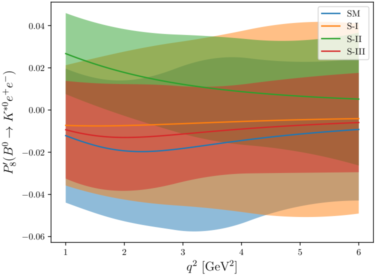
SM
S-I
S-II
S-III
0.04
0.02
0.00
−0.02
−0.04
−0.06
$P_8'(B^0 \to K^{*0}e^+e^-)$
1
2
3
4
5
6
q^2 [GeV^2]

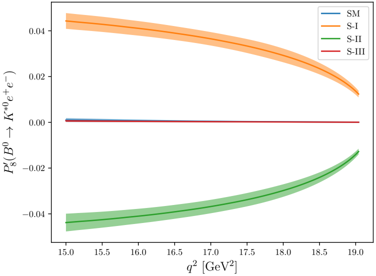
SM
S-I
S-II
S-III
0.04
0.02
0.00
−0.02
−0.04
$P_8'(B^0 \to K^{*0}e^+e^-)$
15.0
15.5
16.0
16.5
17.0
17.5
18.0
18.5
19.0
q^2 [GeV^2]